The Effects of Processing Parameters in the Low-Temperature Chemical Vapor Deposition of Titanium Nitride from Tetraiodotitanium

Cheryl G. Faltermeier, Cindy Goldberg, Michael Jones, Allan Upham, Andreas Knorr, Ana Ivanova, Gregory Peterson, and Alain E. Kaloyeros

New York State Center for Advanced Thin Film Technology and Department of Physics, The University at Albany, State University of New York, Albany, New York 12222, USA

Barry Arkles

Gelest, Incorporated, Tullytown, Pennsylvania 19007, USA

ABSTRACT

Key findings are presented from a systematic study aimed at establishing a fundamental understanding of precursor decomposition pathways and resulting film nucleation and growth kinetics in the chemical vapor deposition of titanium nitride from tetraiodotitanium. As part of the study, key process parameters were varied systematically in order to determine process activation energy and establish corresponding functionality curves for film purity, growth rate, structure, and morphology. The key process parameters studied were substrate temperature, source temperature, hydrogen carrier gas flow, and reactor pressure. Corresponding findings indicated that all four parameters showed a direct and significant effect on film quality. Additionally, a thorough evaluation of resulting film composition, texture, and electrical properties led to the identification of a wide process window for the growth of TiN films with optimized characteristics and performance. In this process window, the TiN films were nitrogen-rich, with iodine concentrations below 2 atom %, displayed resistivities in the range 100 to 150 $\mu\Omega$ cm, depending on thickness, and exhibited excellent step coverage, better than 90% conformality in both nominal 0.45 μm, 3:1 aspect ratio and 0.25 μm, 4:1 aspect ratio contact structures.

Introduction

Current microelectronics technologies employ diffusion barrier layers in the various levels of intrachip metallization schemes to prevent undesirable interactions between the metal plugs and interconnects and surrounding dielectrics. These barrier layers must also serve as strong adhesion promoters to ensure structural integrity of the signal-carrying stacks, in addition to preventing interdiffusion. They also must possess low contact resistivity, be easy to etch, and able to withstand repeated thermal processing.[1]

Titanium/titanium nitride (Ti/TiN) bilayers are presently the most extensively used diffusion barriers/adhesion promoters and are perhaps the most promising for continued use in emerging subquartermicron device generations, at least in the foreseeable future. This is attributed primarily to their desirable physical and chemical properties, as well as the extensive body of knowledge that has already been established across the industry in the areas of reliability and integration of Ti/TiN in chip fabrication flow. However, Ti and TiN are presently deposited by collimated sputtering, a line-of-sight technique unable to meet the step coverage and conformality requirements mandated by the aggressive geometries of subquartermicron technologies.[2]

Chemical vapor deposition, on the other hand, is an attractive alternative, especially in terms of its inherent ability to provide highly conformal profiles in aggressive device topographies. As a result, extensive research and development activities have been dedicated to the optimization of metallorganic and inorganic chemical vapor deposition (CVD) processes for TiN thin films. In metallorganic CVD (MOCVD), the two most commonly investigated organometallic precursors for the deposition of TiN were tetrakisdimethylaminotitanium (TDMAT) and tetrakisdiethylaminotitanium (TDEAT).[3] In particular, experiments[4] using TDEAT were carried out thermally using ammonia as the reactant gas. These experiments demonstrated that stoichiometric TiN films with low levels of carbon and oxygen contamination (<3 atom %) and resistivities of 600 to 800 $\mu\Omega$ cm can be successfully deposited from TDEAT. Unfortunately, films grown in this process regime exhibited a step coverage of only 40 to 50% in 3.4 aspect-ratio contacts. Films with higher step coverage (up to 65%) were also grown by the same thermally activated process using higher precursor-to-ammonia ratios and pressures. However, this process regime caused film resistivity to increase by as much as three orders of magnitude while increasing oxygen concentrations from 3 to 30 atom %.

Experiments done with TDMAT showed a similar tradeoff between film purity and step coverage. Resulting films[5] exhibited step coverage of 75% for 0.4 μm contact vias with 2:1 aspect ratios at a film thicknesses of 150 nm. Just as in the case of TDEAT, these films showed inclusion of N, C, and O with atomic ratios for Ti:N:C:O of 1:1:1.3:1. Corresponding resistivities were high, on the order of 3000 $\mu\Omega$ cm. Further process development has led to step coverage of greater than 80% in a 1.6 × 0.4 μm diam contact.[6] For this process, an in situ postdeposition radio frequency (rf) nitrogen plasma treatment was used to reduce resistivities to values as low as 500 $\mu\Omega$ cm. This reduction in resistivities corresponded to a similar decline in the amount of carbon in the films. Interestingly, no oxygen incorporation was observed, even upon long-term air exposure. Similar results have been reported by Inteman when depositing TiN from both TDMAT and TDEAT using remote plasma CVD.[7]

While these MOCVD processes generate lower levels of particle contamination than the titanium tetrachloride ($TiCl_4$) based inorganic CVD method of growth, their inclusion in emerging subquartermicron device generations appears limited by concerns over MOCVD TiN step coverage in such aggressive structures. Additionally, the need for several cycles of rf N_2-plasma anneals in order to achieve optimum film properties limits the incorporation of this type of process step in production line manufacturing.

For inorganic CVD routes, research has focused on the use of titanium halides, primarily titanium tetrachloride ($TiCl_4$). This compound has been studied extensively for the deposition of TiN, with films grown between 550 and 700 °C containing as little as 1 atom % chlorine, while films grown between 400 and 500 °C exhibit more than 5 atom % chlorine.[8] Excellent step coverage was demonstrated for stoichiometric TiN films. However, serious concerns exist regarding chlorine inclusion in the TiN films due to chlorine's corrosive nature and its resulting effects on the over-

lying metal layers. Thus, chlorine contamination needs to be minimized, requiring the higher temperature regime for this process and thus prohibiting the use of this process above the contact level.

Based on the information presented, it is clear that there is a need for a low-temperature (<450 °C) thermal CVD process for the growth of pure and ultrathin (<250 Å) titanium nitride thin films, which exhibit viable electrical and barrier properties, for incorporation in the 0.18 μm technology and beyond. Accordingly, work herein has focused on the use of a more advantageous precursor, namely, tetraiodotitanium (TiI_4), for the development of a low-temperature TiN CVD process.[9] The proposed approach aims to extend existing technology developed using thermal $TiCl_4$ CVD for deposition of TiN to lower processing temperatures and significantly reduced halide incorporation. More importantly, previous work by the same research group, including diode leakage measurements, has indicated that 2 atom % iodine did not affect TiN performance as a diffusion barrier/adhesion promoter.[10] These findings are consistent with the expectation that the activation energy for iodine diffusion is significantly higher than chlorine, given that I is a much heavier than Cl. It is also supported by work on the interaction of fluorine and chlorine with (111) Si,[11] which showed that the barrier for chlorine penetration into the Si surface is much larger than that for fluorine, a behavior due to the larger size, and hence, ionicity and resulting coulomb interaction of the chlorine atom in comparison with fluorine.

This paper presents the results of a systematic study of precursor decomposition pathways and resulting film nucleation and growth kinetics in TiN CVD from TiI_4. It required varying key process parameters in a systematic fashion in order to determine process activation energy and establish corresponding functionality curves for film purity, growth rate, structure, and morphology. The key process parameters studied were substrate temperature, source temperature, hydrogen carrier gas flow, and reactor pressure. A summary of relevant experimental techniques and methods of analysis is presented below, along with key findings, associated discussions, and pertinent conclusions.

Experimental

The reactor used for these experiments was a custom-made, 8 in. wafer, warm wall, plasma-capable, stainless steel system, while a standard pressure-based bubbler unit was applied to the delivery of the solid TiI_4 precursor. The bubbler was attached to the cone-shaped shower head of the CVD reactor through a delivery line which was designed with a T-shaped section. This section was equipped with two high-vacuum valves to allow precursor delivery to either the processing chamber or through a bypass line to the pumping stack. This bypass line allowed both the establishment of a steady-state precursor flux prior to introduction into the chamber and conditioning of the bubbler prior to deposition. Hydrogen gas was used as carrier gas to aid in precursor delivery.

A cone design was chosen as shower head because of its simplicity and ability to provide good uniformity in precursor and reactant gas distribution over the substrate surface. The top of the cone was equipped with five stainless steel flanges, including two used for connecting the precursor and ammonia (NH_3) delivery lines. Two additional flanges were employed for interfacing the electrical feedthroughs and support for the plasma mesh. The feedthroughs were equipped with ceramic spacers, allowing the plasma mesh to be electrically isolated from the rest of the chamber. The plasma mesh thus acted as active electrode, while the remainder of the system, including the substrate heater chuck, served as ground. The process chamber and delivery lines were kept at temperatures above 140 °C to prevent precursor recondensation.

The substrates were loaded on a heater chuck which consisted of a quartz plate placed on an electrically isolated boroelectric heater. The heater was supported by a stainless steel ring bolted to three ceramic posts which were attached to the base of the reactor. A stainless steel enclosure was used to protect the heater contacts from processing gases. The enclosure was purged with 100 sccm argon (Ar) to prevent diffusion of reactive process gases to the heater connections. Substrate temperature was determined by calibrating the power supplied to the heater as a function of substrate temperature with a specially designed sensor wafer prior to actual processing.

The reactor was symmetrically pumped through its base through four lines. The pumping speed was controlled manually through a Huntington Model GVA600 gate-type throttling valve. The system was equipped with a specialized multitrap which was placed between the reactor and the pumping stack. The three-stage multitrap consisted of a series of water-cooled coils to capture any unreacted precursor, a series of sodasorb filters to neutralize any acidic by-products, and a series of carbon filters. A Stokes Model 070-245 roots blower pumping stack was used during actual deposition runs. The system was also equipped with a Leybold Model 451 high-vaccum turbomolecular pump capable of achieving a base pressure of 10^{-7} Torr. The reactor was leak tested down to 10^{-8} cm^3/min before actual experimentation was started. A Model 128 heated MKS pressure transducer baratron gauge and a Series 421 cold cathode gauge were also attached to this back panel to allow monitoring of reactor pressure.

A load lock was employed to prevent contamination of the process chamber. The load lock was coupled to the chamber using a rectangular Viton O-ring seal and was equipped to handle 200 mm wafers. The load lock was pumped using a Balzers Model TCP121 turbomolecular pumping stack, to a base pressure of 4×10^{-6} Torr. The pressure in the load lock was monitored by an MKS Model 122A pressure transducer baratron gauge at pressures above 10 mTorr and MKS Series 423 cold cathode gauge at pressures below 1 mTorr. The load lock was equipped with a manual, magnetically controlled arm for delivery of the wafer to the heated quartz plate.

A soft hydrogen plasma predeposition clean was performed on all samples prior to deposition. However, no plasma was used during actual deposition. The substrates used for these experiments were nonpatterned silicon and silicon dioxide, Sematech-produced patterned structures with nominal 0.25 μm, 4 to 1 aspect ratio, features, and specialized cantilever structures produced at Stanford. Nonpatterned Si samples were cleaned by rinsing with acetone and then methanol. The substrates were subsequently dried using pure argon gas. Next, the Si samples were placed in a bath of 10% hydrofluoric acid/90% deionized water for 1 min followed by a deionized water rinse in order to remove native oxide. Following the rinse, the substrates were once again dried using pure argon gas. The samples were then mounted on an 8 in. carrier wafer and were heated for a minimum of 10 min prior to deposition. Alternatively, the SiO_2 and patterned samples were rinsed with methanol and then blown dry using pure argon. These samples were also mounted on the same 8 in. carrier wafer as the blanket Si samples prior to the in situ heating step.

As mentioned previously, the effects of the four key process parameters, namely, substrate temperature, source temperature, hydrogen carrier gas flow through the bubbler, and reactor pressure, on key film characteristics were investigated. The relevance of these four parameters, primarily in terms of their effects on film properties, was determined in a screening set of experiments which are beyond the scope of this work and are not discussed here. Each of these parameters was varied singly in order to determine their first-order effects on film quality. In this respect, both the source temperature and hydrogen bubbler flow control the flux of precursor into the reaction zone. Changing the source temperature corresponded to a "coarse change" in precursor flux, while changing the hydrogen bubbler flow served as a "fine" control of precursor flux. The process regime which was investigated for these experiments is listed in Table I. Each experiment

was only performed once. However, a monitor run was reproduced several times during the course of these experiments to ensure process reproducibility.

Methods of Analysis

All TiN samples were characterized at the analytical facilities of the New York State Center for Advanced Thin Film Technology by X-ray photoelectron spectroscopy (XPS), Rutherford backscattering (RBS), atomic force microscopy (AFM), cross-sectional SEM (CS-SEM), and four-point resistivity probe. In these studies, the results were standardized using a pure TiN standard deposited by collimated sputtering at Sematech. Specific details of the analytical methods applied have already been reported and are only summarized here.[10]

Microchemical and compositional information was obtained by XPS and RBS. In addition, RBS was applied in conjunction with CS-SEM in the determination of average growth rates and film thickness. Deposition rates were defined as T/t where T is film thickness and t is run time. Run time was measured starting from the instant when the precursor was actually being delivered into the reactor. Also, a Nanoscope III multimode atomic force microscope was applied to examine the surface morphology of the titanium nitride films. Data was collected in tapping mode AFM with Si cantilevers at resonance frequencies in the range 200 to 300 kHz. Multiple surface locations were probed for each sample using a variety of scan sizes ranging from 500 × 500 nm up to 10 × 10 mm.

Results and Discussion

Effects of processing temperature on growth rates.—The Arrhenius plot of ln (growth rate) vs $1/T$ for our set of experiments is shown in Fig. 1. An increase in the slope is observed at higher temperatures (above 450 °C, corresponding to $1/T$ values below 1.56×10^{-3} K^{-1}), indicating the dominance of a single rate-limiting mechanism. As shown in the following section, film structural and chemical characteristics change once this threshold is crossed. Additionally, the data point at 370 °C (corresponding to a $1/T$ value of 0.00148 K^{-1}) might indicate that a second mechanism is becoming dominant in this region, but more data is necessary from this lower temperature region before a definite conclusion can be reached. This activity is beyond the scope of this work and is discussed in a subsequent report by the authors.

Table I. Process regimes investigated.

NH_3 flow (sccm)	H_2 carrier gas flow (sccm)	Source temperature (°C)	Substrate temperature (°C)	Reactor pressure (Torr)
Hydrogen carrier gas flow series				
400	10	140	420	0.48
400	30	140	420	0.48
400	50	140	420	0.48
400	70	140	420	0.48
400	90	140	420	0.48
Bubbler temperature series				
400	30	90	420	0.48
400	30	100	420	0.48
400	30	110	420	0.48
400	30	120	420	0.48
400	30	140	420	0.48
400	30	145	420	0.48
Substrate temperature series				
400	30	140	370	0.48
400	30	140	420	0.48
400	30	140	440	0.48
400	30	140	460	0.48
400	30	140	490	0.48
Reactor pressure series				
400	30	140	420	0.39
400	30	140	420	0.48
400	30	140	420	0.74
400	30	140	420	0.92
400	30	140	420	1.12

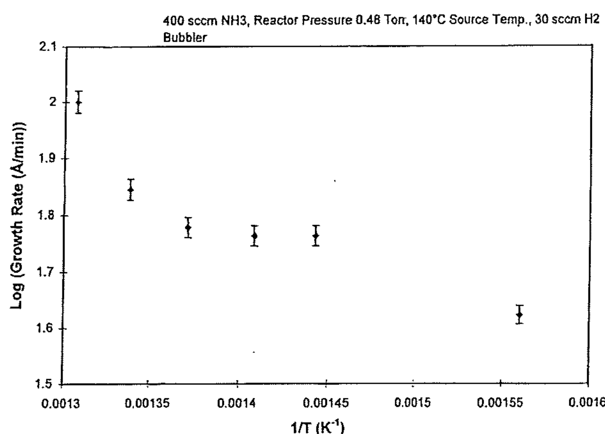

Fig. 1. Arrhenius plot obtained from experiments using TiI_4 as the source chemistry.

The effects of processing temperature on film composition, resistivity, and step coverage.—XPS and RBS were used to investigate the dependence of film composition on processing temperature in the temperature range 370 to 490 °C. All other processing parameters were kept constant, including a 400 sccm NH_3 flow, 0.48 Torr reactor pressure, 30 sccm H_2 carrier gas, and 140 °C source temperature. Given that results on Si and SiO_2 were similar, we discuss only results on Si as the substrate.

Figure 2 displays XPS variations in film concentrations of Ti and N, as well as O and I, as a function of processing temperature. In particular, it is observed that most films grown at substrate temperatures between 370 and 440 °C were stoichiometric TiN within the experimental errors of the techniques used (±10%). XPS depth profile analysis showed that film composition was uniform across its bulk, as shown in Fig. 3. Also, the XPS N ls and Ti $2p_{3/2}$ core energy peaks for the CVD-grown films (Fig. 4) were located at 397.5 and 454.87 eV, respectively. These values are in excellent agreement with their corresponding counterparts from the PVD TiN standard and indicate a N/Ti ratio of ~1. The small peak broadening on the high-energy side of the Ti peak could correspond to a very small titanium oxide phase, which was attributed to oxygen contamination of ≤2 atom %. Iodine incorporation was in the 1 to 2 atom % range. Corresponding step coverage in Sematech nominal 0.25 μm trench structures was better than 90%, as shown in Fig. 5.

At processing temperatures above 450 °C, the films exhibited increased oxygen incorporation with higher substrate temperature, up to ~11 atom % at 490 °C. Iodine levels were below the detection limits of RBS and XPS. The increased oxygen inclusion is not due to a reactor leak, given that it was thoroughly tested and found to be vacu-

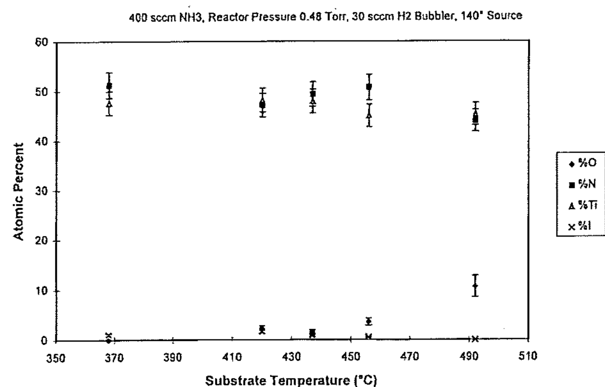

Fig. 2. Composition of TiN films as a function of substrate temperature.

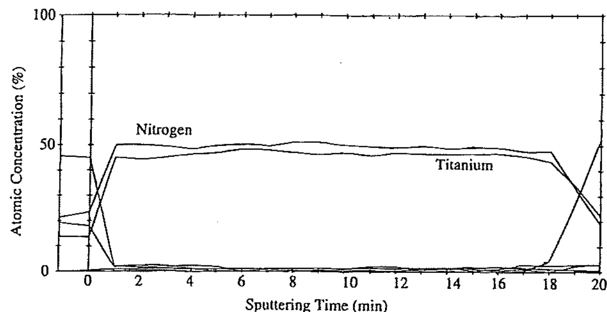

Fig. 3. XPS depth profile of CVD TiN grown at 440 °C susbtrate temperature.

um tight down to 10^{-7} Torr. Instead, it is believed that oxygen is being incorporated in the films through grain boundary diffusion upon exposure to air. This is supported by the following three findings: (*i*) the "open" grain structure observed for the TiN films deposited at higher temperature, as shown in the cross-sectional SEM of Fig. 6 and (*ii*) the surface morphology of the TiN films grown at higher temperature, as documented by the AFM image shown in Fig. 7. AFM supported the CS-SEM findings pertaining to the open TiN structure and yielded a root-mean-square (rms) surface roughness of 6.61 nm for a film thickness of 110 nm.

This surface morphology is significantly different for the TiN films deposited at lower temperatures, as documented in the AFM micrograph of Fig. 8. An AFM surface scan yielded an rms roughness of 1.028 nm in this case (film thickness 90 nm), and (*iii*) the location of the XPS N 1s and Ti $2p_{3/2}$ at 397.5 and 454.87 eV, respectively, in the CVD grown films, similar to the profiles observed in Fig. 4. These peaks correspond to mainly a pure titanium nitride phase.

Film resistivity, on the other hand, varied from ~450 μΩ cm for a 630-nm-thick film grown at 370 °C, down to ~50 μΩ cm for a 1500-nm-thick film deposited at 490 °C. This trend is consistent with the larger role that surface scattering

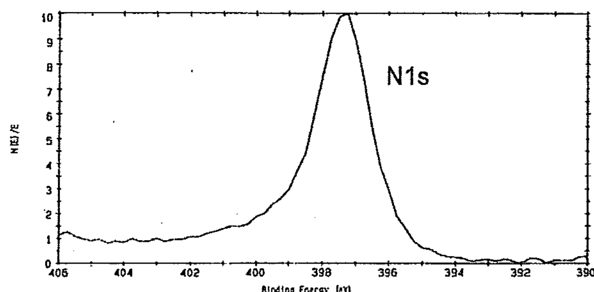

(a)

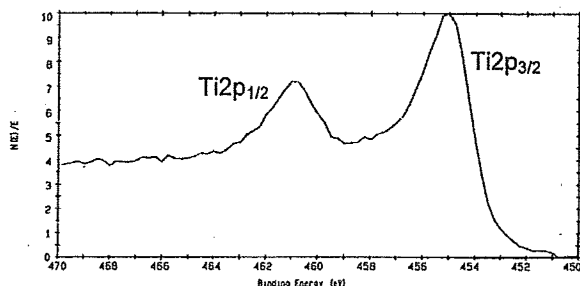

(b)

Fig. 4. XPS scan of (a) N 1s peak and (b) Ti $2p_{3/2}$ peak from CVD TiN film grown at 420 °C substrate temperature.

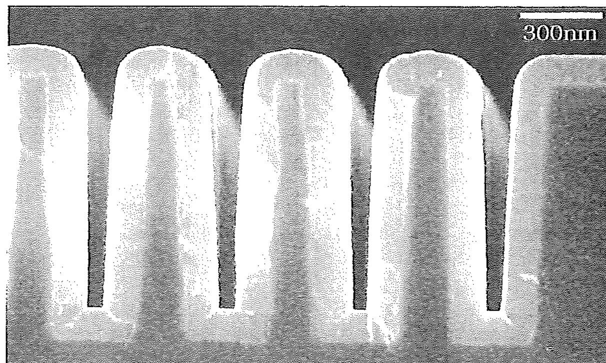

Fig. 5. Cross-sectional SEM of a TiN film grown in a Sematech-nominal 0.25 μm trench at a substrate temperature of 440 °C.

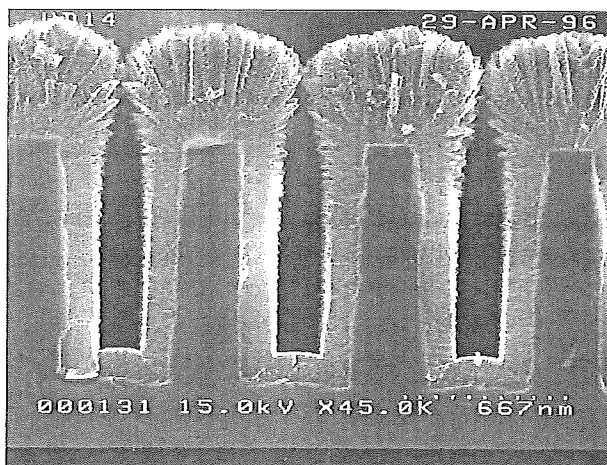

Fig. 6. CS-SEM of a TiN film grown in a 0.5 μm trench at a substrate temperature of 490 °C.

plays with decreasing film thickness, leading to increased film resistivity. Interestingly, the low film resistivity does not seem to be affected by oxygen incorporation at the higher substrate temperatures.

The effect of source temperature on film characteristics.—In CVD processing, varying the source temperature is shown to have a significant effect on precursor flux into the reactor; it provides a "coarse" means to control such flux, with higher source temperature leading to increased precursor flow. Accordingly, work in this section has focused on establishing the role of variations in source temperature, or correspondingly large changes in precursor gas-phase concentration, on resulting film structure, composition, and resistivity.

Figure 9 plots film composition as a function of "coarse" variations in precursor flux. It is observed that films grown at source temperatures below 100 °C exhibit up to 15 atom % oxygen incorporation, which decreases with increasing source temperature to below the detection limits of the analytical techniques employed (XPS and RBS). Interestingly, iodine concentration in the films was also below the detection limits of XPS for source temperatures under 100 °C, and increased slightly to ~1 to 2 atom % for higher temperatures. Corresponding step coverage in Sematech nominal 0.25-μm trench structures was better than 90%, similar to that observed in Fig. 5. Alternatively, the films grown below 100 °C were nitrogen deficient, in contrast to those deposited above that temperature, and were stoichiometric TiN.

The compositional behavior described is consistent with the suggestion that at lower source flux, the TiN films exhibit a less dense structure, which oxidizes upon exposure to air. In this case, oxygen appears to be present not only at grain boundaries, but also at lattice sites with N

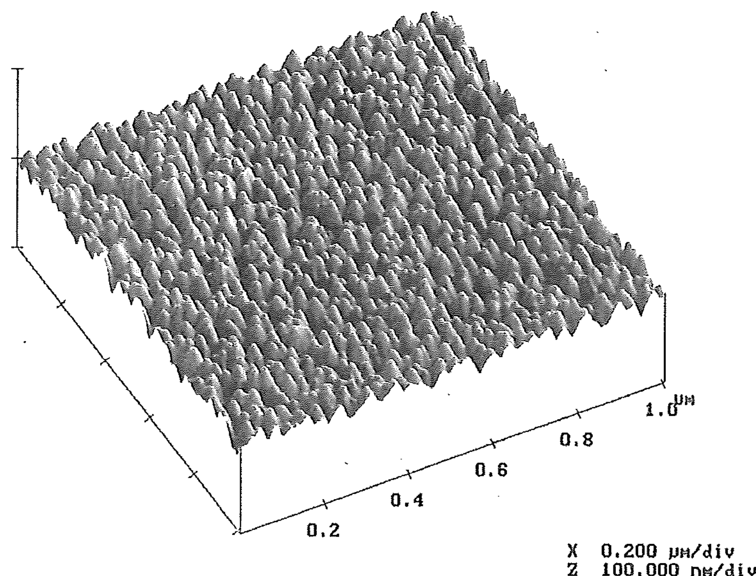

Fig. 7. AFM micrograph of a TiN film grown at 400 sccm NH_3, reactor pressure 0.48 Torr, 490 °C substrate temperature, 140 °C bubbler temperature, and 30 sccm H_2 bubbler flow.

vacancies. This is supported by the following findings: (*i*) the "open" grain structure observed for the TiN films grown at lower source temperature, as shown in the CS-SEM micrograph of Fig. 10; (*ii*) the corresponding TiN surface morphology, as exhibited in the AFM surface map of Fig. 11, which indicates a "looser" surface grain morphology with larger grains and an rms surface roughness of 1.46 nm for a 600-nm-thick film as compared to its higher source temperature counterpart (Fig. 8); (*iii*) the XPS Ti $2p_{3/2}$ core energy peak for the lower source temperature films, indicating the presence of an oxide as well as a nitride phase; and (*iv*) film resistivity behavior as a function of source temperature, as plotted in Fig. 12. Film resistivity is seen to decrease significantly with increasing precursor flux, from ~500 to 1000 μΩ cm for 30 to 50-nm-thick films (T_{source} 90 °C), to below 200 μΩ cm for >100 nm-thick films grown at higher source temperatures. The resistivity values reported for T_{source} < 110 °C are too high to be attributed to film-thickness-driven surface scattering effects. Instead, they could be due to the higher oxygen concentrations observed at the low source temperatures (see Fig. 9).

Similar effects have been observed in CVD TiN from $TiCl_4$.[12,13] TEM analysis of the resulting films also revealed an open grain structure with a large effective surface area. In either case, it is suggested that the lower precursor flux regime causes the formation of a smaller density of surface nucleation sites, which ultimately leads to a larger, less dense, grain structure.

The effect of hydrogen carrier gas flow.—As mentioned earlier, precursor delivery is controlled by two key process

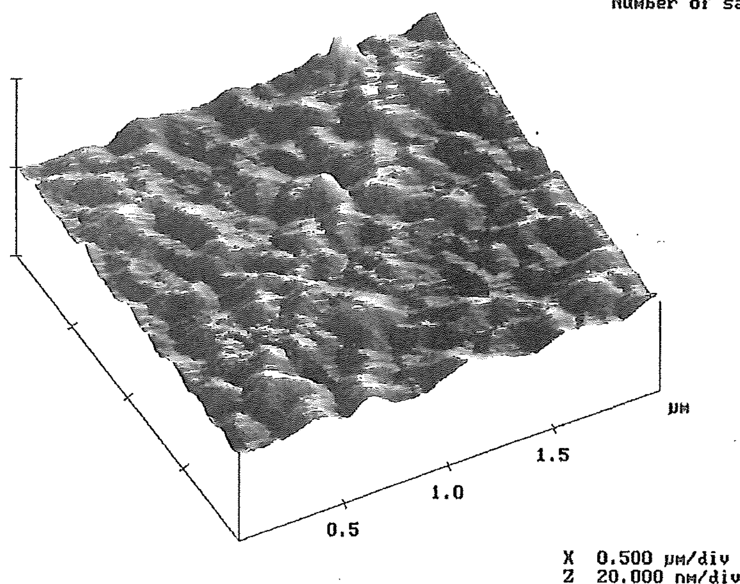

Fig. 8. AFM micrograph of a TiN film grown at 400 sccm NH_3, reactor pressure 0.48 Torr, 420 °C substrate temperature, 140 °C bubbler temperature, and 30 sccm H_2 bubbler flow.

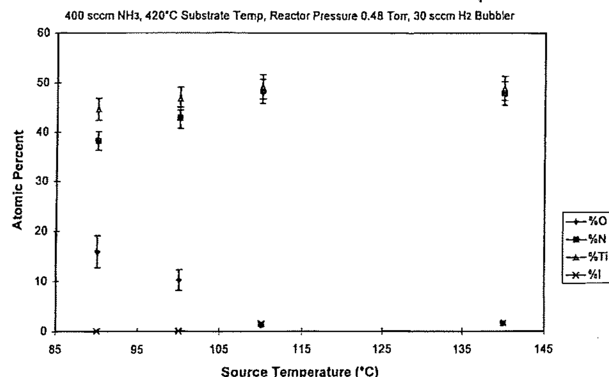

Fig. 9. TiN film composition as a function of source temperature.

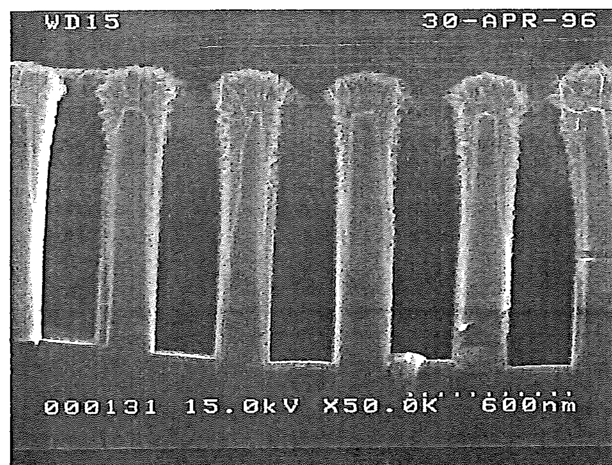

Fig. 10. CS-SEM of a TiN film grown in a 0.3 μm trench at a bubbler temperature of 100 °C.

parameters: source temperature (coarse control of precursor flux) and hydrogen flow through the bubbler (fine control of precursor flux). In this section we discuss the results obtained by varying the amount of hydrogen carrier gas delivered through the bubbler. For this series of experiments, the hydrogen carrier gas flow was varied from 10 to 90 sccm in 20 sccm increments. As expected, most film characteristics showed similar but less dramatic results than those seen by varying the source temperature.

In particular, as in the case of source temperature, films grown with hydrogen flows below 30 sccm show up to 5 atom % oxygen incorporation, which decreased with increasing hydrogen flow to below the detection limits of the analytical techniques used (XPS and RBS). Similarly, I levels were not detectable in films grown at lower hydrogen flows and increased slightly to ~1 to 2 atom % for higher flows. Films grown below 30 sccm H_2 were also nitrogen deficient, in contrast to those grown at higher hydrogen flow, and their resistivity varied from ~500 μΩ cm for 7000-nm-thick films (hydrogen flows 10 sccm), to ~120 μΩ cm for 900-nm-thick films deposited at higher hydrogen flow. As in the case of source temperature, the values reported for hydrogen flow below 30 sccm are too high to be attributed to film-thickness-driven surface scattering effects.

The compositional and conductivity behavior as a function of hydrogen flow ("fine" changes in precursor flux) is in excellent agreement with that seen for source temperature ("coarse" variations in precursor flux) and is attributed to the same structural factors discussed in pevious sections.

The effect of precursor flux on TiN growth rate.—Figure 13 plots TiN growth rate as a function of hydrogen flow. It is observed that higher growth rates are observed for lower hydrogen flow (i.e., smaller precursor flux) in the process regime investigated. An identical trend was observed for growth rates as a function of source temperature. The behavior is similar to that observed in the literature for the dependence of growth rates on $TiCl_4$ partial pressure.[15] In that case, a region of lower precursor flux exists in the pressure range 0.5 to 0.75 Torr, where a dramatic increase in growth rate is observed. Unfortunately, no acceptable explanation is proposed for this increase, but it was suggested that it may be partly due to the gas-phase formation of $TiCl_4$ adducts, which subsequently decompose to yield TiN.[12] A similar explanation could apply in the case of TiI_4.

The effect of reactor pressure.—For the set of experiments described herein, process pressure was varied by controlling pumping speed while maintaining all other processing conditions the same. This was achieved by throttling the gate valve that separated the reactor from

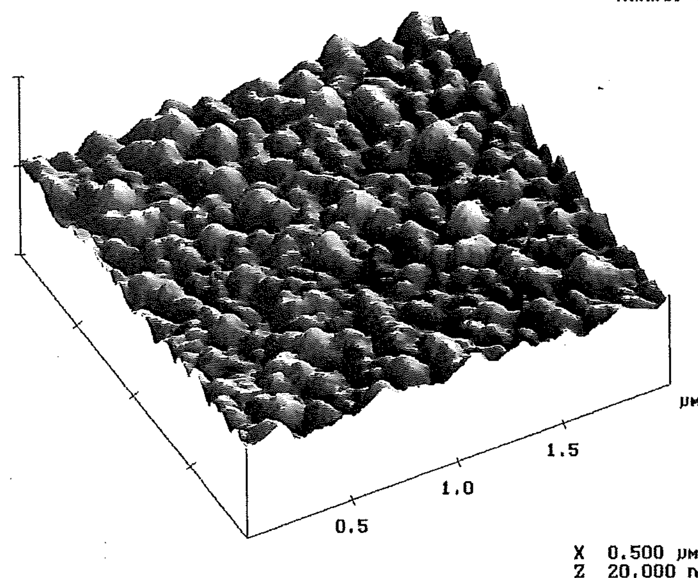

Fig. 11. AFM micrograph of a TiN film grown at 400 sccm NH_3, reactor pressure 0.48 Torr, 420 °C substrate temperature, 90 °C bubbler temperature, and 30 sccm H_2 bubbler flow.

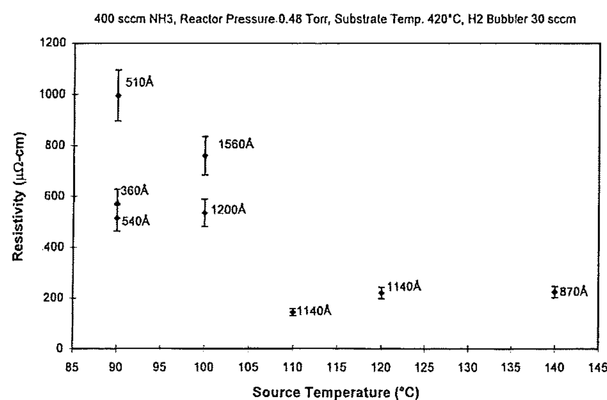

Fig. 12. TiN resistivity vs source temperature.

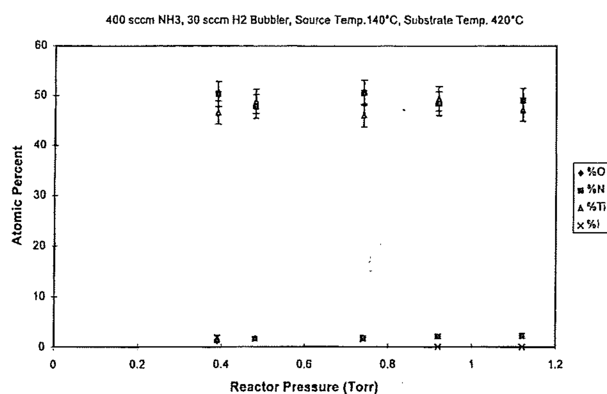

Fig. 14. TiN film composition vs reactor pressure.

the pumping stack, which resulted in increasing reactant residence time in the reaction zone.

Figure 14 plots the effects of processing pressure on the concentrations of N, Ti, I, and O in the films. It is observed that within the experimental errors of the analytical techniques used, film composition was quite constant across the pressure space investigated and corresponded to a stoichiometric TiN phase. Iodine and oxygen concentrations were in the range 1 to 2 atom %, regardless of the processing pressure used. Resistivity measurements indicated that films grown below 1 Torr pressure displayed resistivities below 200 $\mu\Omega$ cm.

However, as pressure was increased above 1 Torr, resistivity was seen to increase dramatically to values in excess of 5000 $\mu\Omega$ cm in the process regime investigated. As discussed earlier, this increase cannot be attributed to I or O contamination, as supported by the XPS Ti 2p and N 1s core energy spectra for the CVD TiN film, indicating a mainly TiN phase with, as discussed before, a small peak broadening on the high-energy side of the Ti peak which corresponded to a very small titanium oxide phase. Instead, this resistivity enhancement is due to the "open" grain structure observed for the TiN films deposited at higher pressure, as shown in the AFM surface grain map of Fig. 15. This morphology results in the incorporation of up to 3 to 4 atom % O in the TiN matrix upon exposure to air, as detected by XPS depth profiling.

One potential explanation for the textural change in TiN at higher processing pressure is possibly the increase in gas-phase reactions in the reaction zone due to the longer reactant residence time in the reactor. In situ quadrupole mass spectrometry (QMS) and Fourier transform infrared spectroscopy (FTIR) investigations of the gas-phase evolution of reactant species should shed some light on the TiN structural behavior.

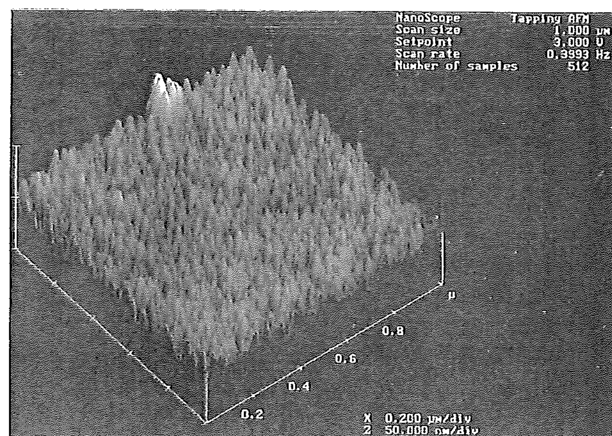

Fig. 15. AFM micrograph of a TiN film grown at 400 sccm NH_3, reactor pressure 0.74 Torr, 420 °C substrate temperature, 140 °C bubbler temperature, and 30 sccm H_2 bubbler flow.

Conclusions

The dependence of film structural, compositional, and electrical properties on key process parameters was investigated in this report through a systematic approach which examined the first-order effects of each parameter singly while maintaining all other parameters constant. In this respect, the key process parameters studied were substrate temperature, source temperature, hydrogen carrier gas flow, and reactor pressure. Resulting findings indicated that each showed a direct and significant effect on film quality. Additionally, it was determined that a wide process window exists for the deposition of nitrogen-rich, gold-colored TiN with I and O levels below 2 atom % and resistivities under 200 $\mu\Omega$ cm. Further investigations are necessary to establish a better understanding of the rate-limiting process steps. FTIR and QMS studies are planned by the Albany group in an effort to achieve this goal.

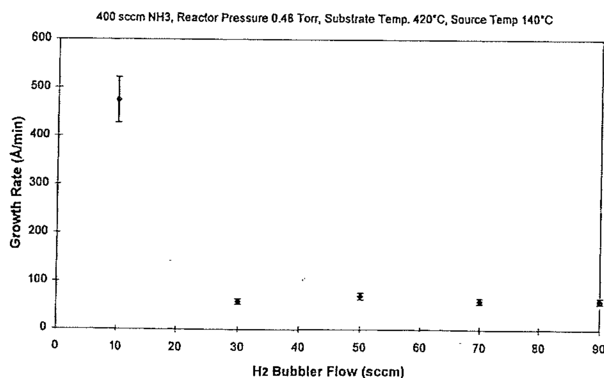

Fig. 13. Growth rate of TiN films vs hydrogen carrier gas flow.

Acknowledgments

The work was supported by Sematech, under its J91 TiN Benchmarking Program, the New York State Center for Advanced Thin Film Technology (CAT), and the National Science Foundation (NSF) Presidential Young Investigator (PYI) Award No. DMR-9157011.

Manuscript submitted April 1, 1997; revised manuscript received September 9, 1997.

The State University of New York at Albany assisted in meeting the publication costs of this article.

REFERENCES

1. G. P. Rao, *Multilevel Interconnect Technology*, McGraw-Hill, Inc., New York (1994).
2. J. Ryan, *MRS Bull.*, **20**, 42 (1995).
3. D. Hoffman, *Polyhedron*, **13**, 1169 (1994).
4. R. Jackson, E. J. McInerney, B. Robers, J. Strupp, A. Belaga, S. Patel, and L. Halliday, in *Advanced Metallization for ULSI Applications in 1994*, R. Blumenthal and G. Janssen, Editors, p 223-229, Material Research Society, Pittsburgh, PA (1995).

5. M. Eizenberg, K. Littau, S. Ghanayem, A. Mak, Y. Maeda, M. Chang, and A. K. Sinha, *Appl. Phys. Lett.*, **65,** 7 (1994).
6. M. Eizenberg, *MRS Bull.,* **20,** 38 (1995).
7. A. Intemann and J. Koerner, *This Journal,* **140,** 3215 (1993).
8. R. Hegde, R Fiordalice, E. Travis, and P. Tobin, *J. Vac. Sci. Technol.,* **B11,** 1287 (1993).
9. C. Goldberg, E. Eisenbraun, S. Komarov, C. Faltermeier, X. Chen, M. Jones, A. Ivanova, R. Fiordalice, F. Pintchovski, B. Arkels, A. Hepp, and A. E. Kaloyeros, in *Advanced Metallization for ULSI Applications X,* R. Blumenthal and G. Janssen, Editors, p 247, MRS, Pittsburgh, PA (1995).
10. C. Faltermeier, C. Goldberg, M. Jones, A. Upham, D. Manger, G. Peterson, J. Lau, A. E. Kaloyeros, B. Arkles, and A. Paranjpe, *This Journal,* **144,** 1002 (1997).
11. M. Seel and P. S. Bagus, *Phys. Rev.,* **B28,** 2023 (1983).
12. M. Buiting, A. Otterloo, and H. Montree, *This Journal,* **138,** 500 (1991).
13. M. Buiting and A. Otterloo, *ibid.,* **139,** 2580 (1992).

Reprinted from Journal of the Electrochemical Society
Vol. 145, No. 2, February 1998
Printed in U.S.A.
Copyright 1998